ENGINEERING JOURNAL

Article

Synthesis and Characterization of the Novel $BiVO_4/CeO_2$ Nanocomposites

Saranyoo Chaiwichian[1], Burapat Inceesungvorn[2], Kanlaya Pingmuang[2], Khatcharin Wetchakun[3], Sukon Phanichphant[4], and Natda Wetchakun[1,*]

1 Department of Physics and Materials Science, Faculty of Science, Chiang Mai University, Chiang Mai 50200, Thailand
2 Department of Chemistry, Faculty of Science, Chiang Mai University, Chiang Mai 50200, Thailand
3 Nanoscience and Nanotechnology Program, Graduate School, Chiang Mai University, Chiang Mai 50200, Thailand
4 Materials Science Research Center, Faculty of Science, Chiang Mai University, Chiang Mai 50200, Thailand
E-mail address: natda_we@yahoo.com*

Abstract. Novel $BiVO_4/CeO_2$ nanocomposites were synthesized by the hydrothermal method combined with the homogeneous precipitation method. The mole ratios of $BiVO_4$:CeO_2 were 0.4:0.6, 0.5:0.5, and 0.6:0.4. The obtained $BiVO_4/CeO_2$ nanocomposites were characterized by X-ray diffraction (XRD) for phase composition and crystallinity. Particle sizes, morphology and elemental composition of $BiVO_4/CeO_2$ nanocomposites were examined by scanning electron microscopy (SEM), transmission electron microscopy (TEM), and energy dispersive X-ray spectroscopy (EDS). The Brunauer, Emmett and Teller (BET) adsorption-desorption of nitrogen gas for specific surface area determination at the temperature of liquid nitrogen was performed on all samples. UV-vis diffuse reflectance spectra (UV-vis DRS) were used to identify the absorption range and band gap energy of the composite catalysts. The results indicated that $BiVO_4/CeO_2$ samples retained monoclinic scheelite and fluorite structures. The morphologies of nanocomposite samples consisted of rod-like, plate-like and spheroidal shapes. Specific surface area (SSA_{BET}) of the novel synthesized catalysts drastically increased from 38–62 m^2/g whereas an average BET-equivalent particle diameter (d_{BET}) significantly decreased from 30–12 nm, upon increasing the amount of CeO_2 in the $BiVO_4/CeO_2$ composite. The absorption spectra of all nanocomposite samples were shifted to the visible region, suggesting the potential application of this novel composite as an active visible-light driven photocatalyst.

Keywords: $BiVO_4$, CeO_2, characterization, nanocomposites, synthesis.

ENGINEERING JOURNAL Volume 16 Issue 3
Received 19 November 2012
Accepted 15 February 2012
Published 1 July 2012
Online at http://www.engj.org/
DOI:10.4186/ej.2012.16.3.153

This paper is based on the poster presentation at the German-Thai Symposium on Nanoscience and Nanotechnology 2011—Green Nanotechnology of the Future, GTSNN 2011, in Nakhon Ratchasima, Thailand, 13-16 September 2011.

DOI:10.4186/ej.2012.16.3.153

1. Introduction

Water cleaning applications of heterogeneous photocatalysis have been widely investigated in the past 10 years [1]. Photocatalytic activity of cerium dioxide (CeO_2) with wide band gap energy of 3.2 eV has been intensively studied under UV irradiation due to its non-toxicity, low cost, and chemical stability [2–3]. However, the broad band gap energy of this metal oxide limits its further use in solar light and visible light [4]. Therefore, many researches have been focused on narrowing the band gap energy of CeO_2 photocatalyst [5]. This can be done either by doping CeO_2 with metal/non-metal elements or forming the heterojunction between CeO_2 and a narrow band gap semiconductor. By using coupled semiconductor photocatalyst, improved charge separation and thus enhanced photocatalytic activity due to high efficiency of the interfacial charge transfer can be obtained [6]. Therefore, our present study has been devoted to the synthesis of CeO_2-based composite catalyst with visible-light photoactivity.

A narrow band gap metal oxide used to couple with CeO_2 in this work is bismuth vanadate ($BiVO_4$). $BiVO_4$ has been chosen as a sensitizer due to its high visible-light absorption ability. Normally, $BiVO_4$ exists in three crystalline phases which are monoclinic scheelite, tetragonal zircon and tetragonal scheelite. Among those three crystalline forms, the monoclinic $BiVO_4$ structure was reported to show high photocatalytic activity under visible light irradiation due to its relatively narrow band gap energy of 2.4 eV, compared to the two tetragonal phases with the band gap energy of 3.1 eV [7]. Therefore, the formation of monoclinic $BiVO_4$ phase is preferable with an expectation to shift the photoactivity of CeO_2 into visible-light region and thus enhanced photocatalytic efficiency could be obtained. To the best of our knowledge, preparation and characterization of $BiVO_4/CeO_2$ composite have not been previously reported, therefore this work aims to synthesize and elucidate the physical and optical properties of this novel composite material. Many methods used for composite synthesis include hydrothermal treatment, solid state reaction, precipitation, sol-gel, and sonochemical synthesis [8–17].

In the present study, novel $BiVO_4/CeO_2$ nanocomposites with different $BiVO_4$:CeO_2 mole ratios were synthesized by the homogeneous precipitation coupled with hydrothermal method. The mole ratio between CeO_2 and $BiVO_4$ was varied in order to obtain the most suitable composite material used for further application as photocatalyst These processes demonstrated good reproducibility for synthesis of novel $BiVO_4/CeO_2$ nanocomposites. In addition, the hydrothermal process used in this work also provides many advantages such as one-step synthesis of nanomaterials, removal of the complicated calcination step, uniform small particle size, high purity product formation and an environmentally friendly synthesis method.

2. Experimental

2.1. Synthesis of $BiVO_4/CeO_2$ Nanocomposites

Pure CeO_2 was firstly synthesized by the homogeneous precipitation method using cerium (III) nitrate hexahydrate ($Ce(NO_3)_3{\cdot}6H_2O$) as a cerium precursor. Cerium (III) nitrate hexahydrate 10.9078 g was dissolved in 80% ethylene glycol solution and heated at 50°C until a homogeneous solution was obtained. When the temperature was constant at 50°C, 25 mL of 3.0 M ammonia solution was added dropwise. The obtained suspension was then centrifuged at 5000 rpm for 10 min, washed with deionized water 3 times and then dried in an oven at 80°C for 24h. The powder was subsequently calcined in a furnace at a temperature of 500°C for 1h and finally pure CeO_2 was obtained.

Hydrothermal method was employed to synthesize high purity bismuth vanadate ($BiVO_4$) particle by using bismuth nitrate ($Bi(NO_3)_3{\cdot}6H_2O$) and ammonium vanadate ($(NH_4)VO_3$) as precursors. The solution of bismuth nitrate and ammonium vanadate in 1:1 mole ratio was homogeneously mixed. Then ammonium hydroxide was added dropwise into the previously mixed solution until pH 7 was obtained. Finally, the solution mixture was treated at 120°C for 6h in Teflon-lined stainless steel autoclave. The yellow precipitate was finally dried at 80°C for 24h.

The homogeneous precipitation coupling with the hydrothermal process was employed for the synthesis of $BiVO_4/CeO_2$ nanocomposites with $BiVO_4$:CeO_2 mole ratios of 0.4:0.6, 0.5:0.5, and 0.6:0.4. The nanocomposite of $BiVO_4/CeO_2$ was obtained by mixing the solution of bismuth nitrate and ammonium vanadate with the previously prepared CeO_2 powders and then the solution pH was adjusted to 7. The solution was subsequently transferred into Teflon-lined stainless steel autoclave and hydrothermal

reaction was carried out at 120°C for 6h. Finally, $BiVO_4/CeO_2$ nanocomposites were obtained from centrifugation and drying at 80°C for 24h.

2.2. Characterization

Optical absorbance spectra of the samples were obtained from a doubled-beam UV-vis spectrophotometer equipped with an integrating sphere (UV-vis, Lambda 950). The crystalline phase and crystallite sizes of $BiVO_4$ nanoparticle, CeO_2 nanoparticle and $BiVO_4/CeO_2$ nanocomposites were determined by powder X-ray diffraction analysis (XRD, Philips X'Pert MPD). The crystallite sizes of pure $BiVO_4$ nanoparticle, pure CeO_2 nanoparticle and $BiVO_4/CeO_2$ nanocomposites were evaluated according to Scherrer equation $L=K\lambda/(\beta\cos\theta)$, where L is crystallite size, λ is the wavelength of X-ray radiation (CuK_α = 0.15406 nm), K is a constant taken as 0.89, β is the full width at half maximum (FWHM) and θ is the diffraction angle at the maximum intensities. Brunauer-Emmett-Teller (BET, Adtosorb 1 MP, Quantachrome) surface areas of the materials were analyzed by nitrogen adsorption-desorption measurement. The morphologies, microstructures, and elemental composition of the as-prepared samples were characterized by scanning electron microscopy (SEM, JEOL JSM-5910LV and JEM-6335F) and energy-dispersive X-ray spectroscopy (EDS) analysis. The morphologies and actual size of all samples were analyzed by transmission electron microscopy (TEM, JEOL JEM-2010). Isoelectric points (IEP) of $BiVO_4$ and CeO_2 nanoparticles were also examined by zetasizer nano instrument (ZS Malvern).

3. Results and Discussion

3.1. UV-vis Diffuse Reflectance Spectrophotometry Analysis

Figure 1 shows the UV-vis spectra of pure $BiVO_4$ nanoparticle, pure CeO_2 nanoparticle and different mole ratios of $BiVO_4$:CeO_2 nanocomposites varying from 0.4:0.6 to 0.6:0.4. The relationship between absorption coefficient (a) and incident photon energy ($h\upsilon$) can be described as Eq. (1) [7].

$$(ah\upsilon) = A(h\upsilon - E_g)^{1/2} \quad (1)$$

where A, E_g and $h\upsilon$ represent constant, the direct band gap energy and incident photon energy, respectively. The onset absorption edges and band gap energies of pure $BiVO_4$ nanoparticle, pure CeO_2 nanoparticle and $BiVO_4/CeO_2$ nanocomposites are shown in Fig. 1(a) and (b). The optical band gap of crystalline semiconductor was estimated by the straight-line intercept fitted to a graph from a plot of $(ah\upsilon)^2$ versus photo energy ($h\upsilon$) as shown in Fig. 1(b). The results indicated that absorption edges of all $BiVO_4/CeO_2$ nanocomposites were quite similar to each other. However, different absorption band gaps, corresponding to 2.49, 2.77 and 2.46 eV, were observed in the case of pure $BiVO_4$ nanoparticle, pure CeO_2 nanoparticle and $BiVO_4/CeO_2$ nanocomposites, respectively. Therefore, with the use of the $BiVO_4/CeO_2$ composite, enhanced photocatalytic degradation activity in visible-light region is likely obtained. A decrease in band gap energy together with an enhanced absorption intensity of the composite material upon increasing the amount of $BiVO_4$ has been observed as seen from the UV-vis results in Fig. 1. This phenomenon could be due to many factors such as morphology, crystallite size, phase structure and amount of $BiVO_4$ as previously described in Ref. [18-20]. Therein, various sizes and morphologies of $BiVO_4$ such as flower-like, plate-like and cuboid-like shapes exhibited different band gap energies and optical absorbance values. These differences were ascribed to i) the specific configuration of sample morphology, especially the hierarchical configuration. Since multiple scattering of UV-vis light within the hierarchical framework could lead to a long optical path length for light transport and an enhanced absorbance and ii) different sizes of $BiVO_4$ (larger particle size would lead to narrower band gap energy).

DOI:10.4186/ej.2012.16.3.153

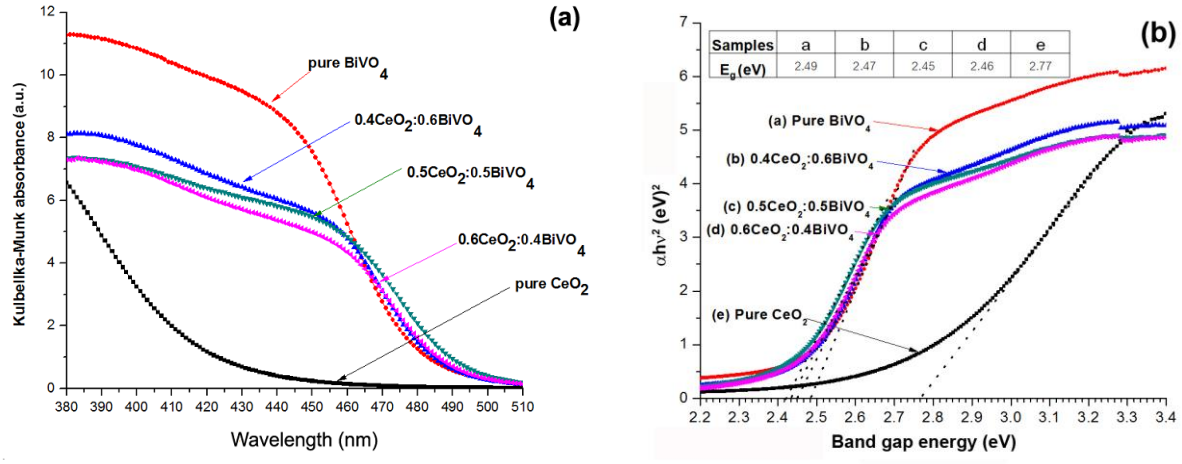

Fig. 1. (a) Kubelka-Munk absorbance plot (b) band gap energy of pure $BiVO_4$ nanoparticle, pure CeO_2 nanoparticle and $BiVO_4/CeO_2$ nanocomposites with different $BiVO_4$:CeO_2 mole ratios.

3.2. XRD Patterns Analysis

Figure 2 shows the XRD patterns of pure $BiVO_4$ nanoparticle, pure CeO_2 nanoparticle and novel $BiVO_4/CeO_2$ nanocomposites. The XRD peaks of pure CeO_2 at 2θ of 28.8°, 33.3°, 47.6°, and 56.4° were respectively indexed as (111), (200), (220), and (311) planes of fluorite structure according to the Joint Committee Powder Diffraction Standards (JCPDS) file no. 081-0792. While the diffraction peaks of pure $BiVO_4$ at 2θ of 28.8°, 30.5°, 34.5°, 35.2°, 39.8°, and 42.5° were respectively indexed as (112), (004), (200), (020), (211), and (015) planes of monoclinic $BiVO_4$ structure according to JCPDS file no. 014–0688. It can be seen that the monoclinic structure was a predominant phase whereas the tetragonal structure presented as a minor component in the composite sample. Diffraction patterns of $BiVO_4/CeO_2$ nanocomposites showed the combination of XRD profiles of both CeO_2 and $BiVO_4$ nanoparticles structures. The average crystallite sizes of pure $BiVO_4$ nanoparticle, pure CeO_2 nanoparticle and $BiVO_4/CeO_2$ nanocomposites calculated by Scherrer equation were found to be 30, 6 and 19–22 nm, respectively. Diffraction peaks of $BiVO_4/CeO_2$ nanocomposites were broader upon increasing CeO_2 amount in the samples. This indicated the existence of smaller particle sizes in the nanocomposite containing high CeO_2 content.

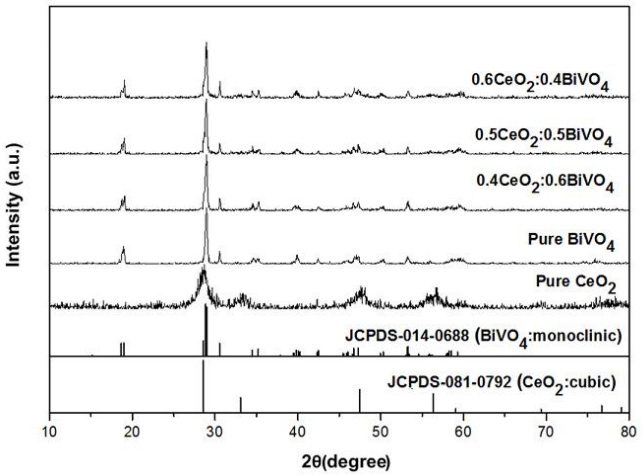

Fig. 2. X-ray diffraction patterns of pure $BiVO_4$ nanoparticle, pure CeO_2 nanoparticle and $BiVO_4/CeO_2$ nanocomposites in different $BiVO_4$:CeO_2 mole ratios.

3.3. BET-Specific Surface Area Analysis

BET specific surface areas (SSA_{BET}) of pure $BiVO_4$ nanoparticle, pure CeO_2 nanoparticle and $BiVO_4/CeO_2$ nanocomposites are shown in Fig. 3 together with the BET particle diameters (d_{BET}) which have been calculated by using the formula as follows:

$$d_{BET} = 6/(\varrho_{BiVO4} \times SSA_{BET} \times wt\%BiVO_4 + \varrho_{CeO2} \times SSA_{BET} \times wt\%CeO_2)$$

ϱ_{BiVO4} and ϱ_{CeO2} are the weight densities of $BiVO_4$ (5.90 g/cm^3) and CeO_2 (7.215 g/cm^3), respectively. Pure $BiVO_4$ nanoparticle and pure CeO_2 nanoparticle were found to have SSA_{BET} of 13 and 150 m^2/g which corresponded to the BET equivalent diameter of 75 and 5 nm, respectively. In the case of $BiVO_4/CeO_2$ nanocomposites, the results clearly showed that upon increasing the amount of CeO_2 in the samples, specific surface area were drastically increased from 38–62 m^2/g whereas the average BET-equivalent particle diameter decreased from 30–12 nm, respectively. Since the particle diameter obtained from BET method is an average value [21], therefore increasing amount of CeO_2 which possesses small particle size in the composite sample could possibly lead to a decrease in an average BET particle diameter.

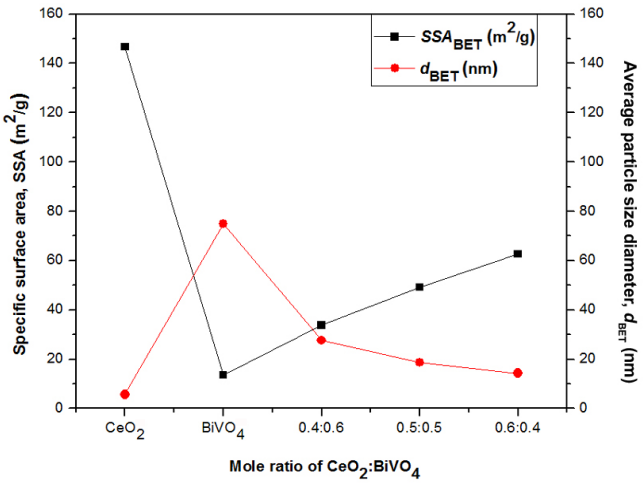

Fig. 3. BET Specific surface areas of pure $BiVO_4$ nanoparticle, pure CeO_2 nanoparticle and $BiVO_4/CeO_2$ nanocomposites in different $BiVO_4$:CeO_2 mole ratios.

3.4. Morphology and Microstructure

The morphology and particle size of all samples were investigated by scanning electron microscopy and transmission electron microscopy. Fig. 4 (a), (b) and (c) shows the SEM images of pure $BiVO_4$ nanoparticle, pure CeO_2 nanoparticle and $0.6BiVO_4$:$0.4CeO_2$ nanocomposites. Pure $BiVO_4$ exhibited in rod-like and plate-like shapes whereas pure CeO_2 presented in only spherical shape. So, $BiVO_4/CeO_2$ nanocomposites reveal in three mixing shapes involving rod-like plate-like and spherical. Nevertheless, the presence of very small spherical-like CeO_2 can be found from the TEM image in Fig. 5(c). Accurate sizes and morphologies of the obtained samples were further investigated by TEM analysis. EDS spectrum of $0.6BiVO_4$:$0.4CeO_2$ nanocomposites (Fig. 4(d)) also indicated the existence of Bi, V, Ce and O elements in the sample. EDS spectrum of $0.6BiVO_4$:$0.4CeO_2$ nanocomposites (Fig. 4(d)) also indicated the existence of Bi, V, Ce and O elements in the sample.

DOI:10.4186/ej.2012.16.3.153

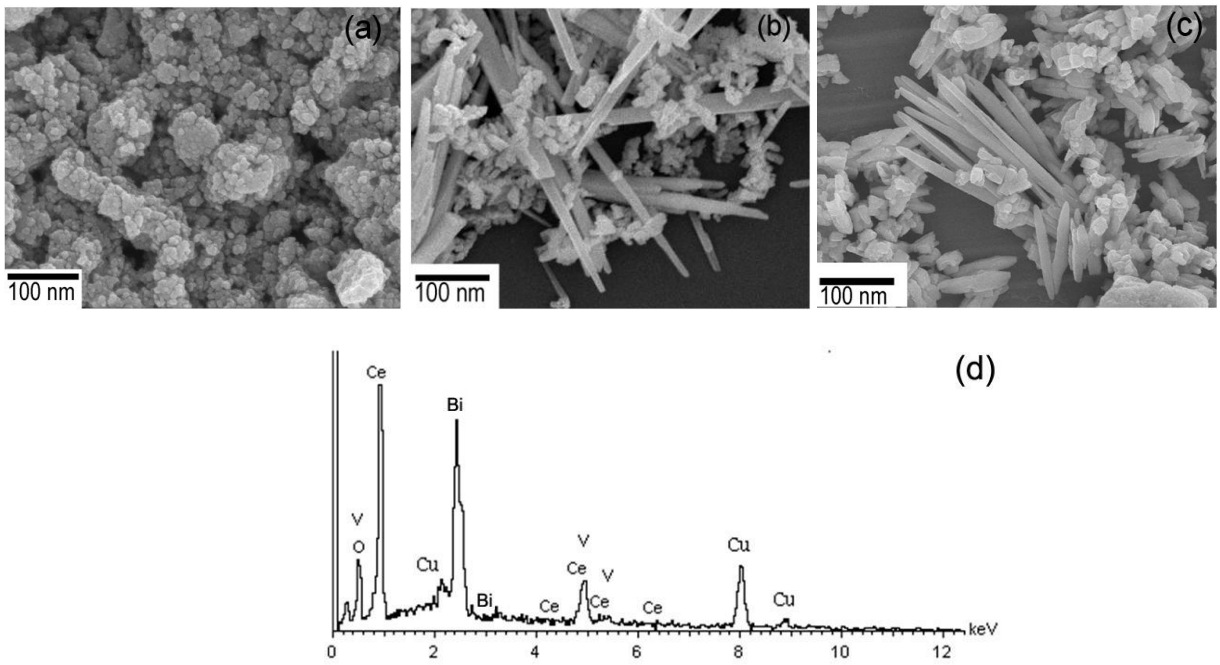

Fig. 4. SEM images of (a) pure CeO_2 nanoparticle, (b) pure $BiVO_4$ nanoparticle and (c) 0.6 $BiVO_4$:0.4 CeO_2 nanocomposite and (d) EDS of (c).

TEM images as presented in Fig. 5 showed the spherical morphology of CeO_2 with particle diameter ranging from 5–10 nm. The size of rod-like $BiVO_4$ was found to be 20–50 nm in diameter and 10–20 μm in length whereas the size of plate-like $BiVO_4$ was about 100–200 nm. Fig. 5 (c) shows the presence of CeO_2 particles deposited on $BiVO_4$ surface possibly due to electrostatic attraction as supported by our isoelectric point (IEP) study. The isoelectric points of CeO_2 and $BiVO_4$ nanoparticles examined by zeta potential were found to be 7.33 and 4.36 respectively. The IEP results suggested that CeO_2 and $BiVO_4$ possess surface positive and negative charges respectively, under the preparation condition of pH 7 which was use in this work. Electron diffraction patterns of pure $BiVO_4$ nanoparticle, pure CeO_2 nanoparticle and $0.6BiVO_4$:$0.4CeO_2$ nanocomposites, showing as insets of Figs. 5 (a), (b) and (c), revealed polymorphic discrete rings of the crystalline materials. The obtained spot ring type of selected area electron diffraction (SAED) pattern indicated that crystals oriented in a number of different directions. Brightness of the ring patterns observed from all samples indicated quite high degree of crystallinity in polycrystals. Radius distance between the rings in electron diffraction patterns was used for determination of lattice *d*-spacing from equation $\lambda L=Rd$, where; λL is camera constant (24.9630 mm Å) and *R* is the radius from the centre of the inner ring to the next ring. The lattice *d*-spacing of pure CeO_2 nanoparticle and pure $BiVO_4$ nanoparticle calculated from electron diffraction patterns corresponded very well with JCPDS powder diffraction file no. 081–0792 for CeO_2 and 014–0688 for monoclinic $BiVO_4$. The calculated lattice spacing of pure CeO_2 (Fig. 5(a)) and pure $BiVO_4$ (Fig. 5(b)) from SAED analysis were 3.12, 2.70, 1.92, and 1.63 Å which correspond to the (111), (200), (220), and (311) planes of CeO_2 and 4.75 and 2.92 Å, to the (110) and (040) planes of $BiVO_4$, respectively [22, 23]. The SAED pattern of $BiVO_4/CeO_2$ (Fig. 5(c)) shows a defined spot pattern, suggesting the single crystal character of the as-synthesized $BiVO_4/CeO_2$. Results from electron diffraction analysis were very well in agreement with those from XRD study.

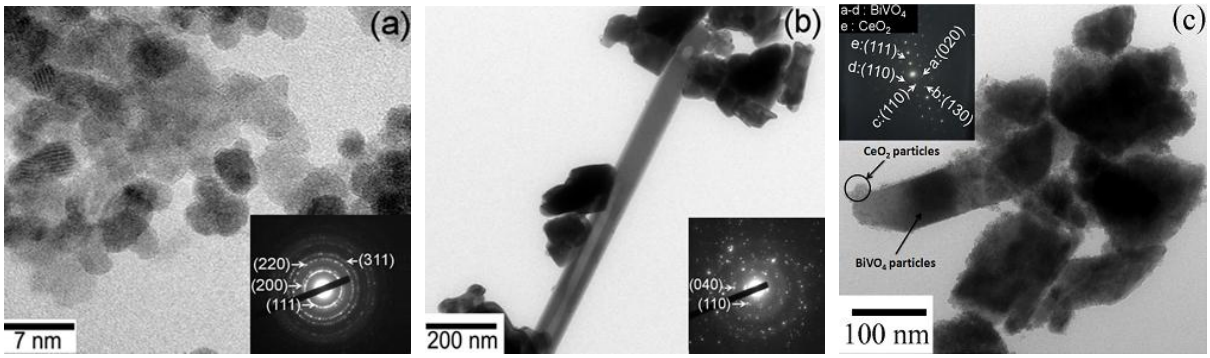

Fig. 5. TEM images and electron diffraction patterns (shown as insets) of (a) pure CeO_2 nanoparticle, (b) pure $BiVO_4$ nanoparticle and (c) $0.6BiVO_4$:$0.4CeO_2$ nanocomposite.

4. Conclusions

The novel $BiVO_4/CeO_2$ nanocomposites were successfully prepared by the homogeneous precipitation combined with the hydrothermal method. $BiVO_4/CeO_2$ nanocomposite in all compositions shifted the absorption onset towards a visible region. Therefore, this novel $BiVO_4/CeO_2$ nanocomposite is likely to be an effective visible-light driven photocatalyst. The XRD diffraction peaks of $BiVO_4/CeO_2$ nanocomposites corresponded to JCPDS file no. 014–0688 of $BiVO_4$ and JCPDS file no.081–0792 of CeO_2. The specific surface area of $BiVO_4/CeO_2$ nanocomposite increased upon increasing amount of CeO_2 in the composite material. BET specific surface areas (SSA_{BET}) of the synthesized samples were found to be in the range of 13–150 m^2/g and the BET particle diameters were in the range of 5–75 nm. SEM results clearly showed that $BiVO_4/CeO_2$ nanocomposites were spherical, rod-like and plate-like in shape. According to TEM results, the size of rod-like $BiVO_4$ was found to be 20–50 nm in diameter and 10–20 μm in length whereas the size of plate-like $BiVO_4$ was about 100–200 nm. The particle size of spherical CeO_2 was in the range 5–10 nm in diameter.

Acknowledgements

This work was supported financially by the National Metal and Materials Technology Center (MTEC), the National Science and Technology Development Agency (NSTDA), Ministry of Science and Technology Grant (MT-B-53-CER-10-270-G); the National Research University Project under Thailand's Office of the Higher Education Commission, Materials Science Research Center; the Thailand Research Fund (TRF) and the Commission on Higher Education (CHE) Grant (MRG5480255); Department of Chemistry and Department of Physics and Materials Science, Faculty of Science, the Graduate School, Chiang Mai University.

References

[1] L. F. Liotta, M. Gruttadauria, G. Di Carlo, G. Perrini, and V. Librando, "Heterogeneous catalytic degradation of phenolic substrates:catalysts activity," *J. Hazard. Mater.,* vol. 162, pp. 588–606, Mar. 2009.

[2] L. Truffault, M.-T. Ta, T. Devers, K. Konstantinov, V. Harel, C. Simmonard, C. Andreazza, I. P. Nevirkovets, A. Pineau, O. Veron, and J.-P. Blondeau, "Application of nanostructured Ca doped CeO_2 for ultraviolet filtration," *Mater. Res. Bull.*, vol. 45, pp. 527–535, May 2010.

[3] L. Zhou, W. Wang, S. Liu, L. Zhang, H. Xu, and W. Zhu, "A sonochemical route to visible-light-driven high-activity $BiVO_4$ photocatalyst," *J. Mol. Catal. A: Chem.*, vol. 252, pp.120–124, June 2006.

[4] H. Li, G. Liua, and X. Duana, "Monoclinic $BiVO_4$ with regular morphologies: hydrothermal synthesis, characterization and photocatalytic properties," *Mater. Chem. Phys.*, vol. 115, pp. 9–13, May 2009.

[5] P. Chatchai, Y. Murakami, S. Kishioka, A. Y. Nosaka, and Y. Nosaka, "Efficient photocatalytic activity of water oxidation over $WO_3/BiVO_4$ composite under light irradiation," *Electrochim. Acta.*, vol. 54, pp. 1147–1152, Jan. 2009.

[6] S. Hu, F. Zhou, L. Wang, and J. Zhang, "Preparation of Cu_2O/CeO_2 heterojunction photocatalyst for the degradation of acid orange 7 under visible light irradiation, *Catal. Commun.*, vol. 12, pp. 794–797, Apr. 2011.

[7] A. Zhang and J. Zhang, "Hydrothermal processing for obtaining of $BiVO_4$ nanoparticles," *Mater. Lett.*, vol. 63, pp. 1939–1942, Sept. 2009.

[8] P. Ji, J. Zhang, F. Chen, and M. Anpo, "Study of adsorption and degradation of acid orange 7 on the surface of CeO_2 under visible light irradiation," *Appl. Catal. B: Environ.*, vol. 85, pp. 148–154, Jan. 2009.

[9] L. Qian, J. Zhu, W. Du, and X. Qian, "Solvothermal synthesis, electrochemical and photocatalytic properties of monodispersed CeO_2 nanocubes," *Mater. Chem. Phys.*, vol. 115, pp. 835–840, June 2009.

[10] H.-Q. Jiang, H. Endo, H. Natori, M. Nagai, and K. Kobayashi, "Fabrication and efficient photocatalytic degradation of methylene blue over $CuO/BiVO_4$ composite under visible-light irradiation," *Mater. Res. Bull.*, vol. 44, pp. 700–706, Mar. 2009.

[11] M. Shang, W. Wang, L. Zhou, S. Sun, and W. Yin, "Nanosized $BiVO_4$ with high visible-light-induced photocatalytic activity: ultrasonic-assisted synthesis and protective effect of surfactant," *J. Hazard. Mater.*, vol. 172, pp. 338–344, Dec. 2009.

[12] L. Zhou, W. Wang, S. Liu, L. Zhang, H. Xu, and W. Zhu, "A sonochemical route to visible-light-driven high-activity $BiVO_4$ photocatalyst," *J. Mol. Catal. A: Chem.*, vol. 252, pp. 120–124, June 2006.

[13] J. Yu, Y. Zhang, and A. Kudo, "Synthesis and photocatalytic performances of $BiVO_4$ by ammonia co-precipitation process", *J. Solid State Chem.*, vol. 182, pp. 223–228, Feb. 2009.

[14] S. Kohtani, J. Hiro, N. Yamamoto, A. Kudo, K. Tokumura, and R. Nakagaki, "Adsorptive and photocatalytic properties of Ag-loaded $BiVO_4$ on the degradation of 4-*n*-alkylphenols under visible light irradiation", *Catal. Commum.*, vol. 6, pp. 185-189, July 2005.

[15] M. Long, W. Cai, J. Cai, B. Zhou, X. Chai, andY. Wu, "Efficient photocatalytic degradation of phenol over $Co_3O_4/BiVO_4$ composite under visible light irradiation", *J. Phys. Chem.*, vol. 110, pp. 20211–20216, July 2006.

[16] T. Yang, D. Xia, G. Chen, and Y. Chen, "Influence of the surfactant and temperature on the morphology and physico-chemical properties of hydrothermally synthesized composite oxide $BiVO_4$", *Mater. Chem. Phys.,* vol. 114, pp. 69–72, Mar. 2009.

[17] S. Tokunagu, H. Kato, and A. Kudo, "Selective preparation of monoclinic and tetragonal $BiVO_4$ with scheelite structure and their photocatalytic properties", *Chem. Mater.,* vol. 13, pp. 4624–4628, Jan. 2001.

[18] H. Li, G. Liu, and X. Duan, "Monoclinic $BiVO_4$ with regular morphologies: hydrothermal synthesis, characterization and photocatalytic properties," *Mater. Chem. Phys.*, vol. 115, pp. 9–13, Jan. 2009.

[19] S. Liu and J. Yu, "Cooperative self-construction and enhanced optical absorption of nanoplates-assembled hierarchical Bi_2WO_6 flowers," *J. Solid State Chem.*, vol. 181, pp. 1048–1055, Mar. 2008.

[20] J. Yu, Y. Su, B. Cheng, and M. Zhou, "Effects of pH on the microstructures and photocatalytic activity of mesoporous nanocrystalline titania powders prepared via hydrothermal method," *J. Mol. Catal. A: Chem.*, vol. 258, pp. 104–112, Oct. 2008.

[21] H. D. Jang, S.-K. Kim, and S.-J. Kim, "Effect of particle size and phase composition of titanium dioxide nanoparticles on the photocatalytic properties," *J. Nanopart. Res.*, vol. 3, pp. 141–147, Mar. 2001.

[22] K. Nakagawa, Y. Murata, M. Kishida, M. Adachi, M. Hiro, and K. Susa, "Formation and reaction activity of CeO_2 nanoparticles of cubic structure and various shaped CeO_2-TiO_2 composite nanostructures," *Mater. Chem. Phys.*, vol. 104, pp. 30–39, Feb. 2007.

[23] D. Ke, T. Peng, L. Ma, P. Cai, and P. Jiang, Photocatalytic water splitting for O_2 production under visible-light irradiation on BiVO4 nanoparticles in different sacrificial reagent solutions, *Appl. Catal A: Gen.*, vol. 350, pp. 111–117, Aug. 2008.